water

MDPI

Article

Design and Properties of Titanium Dioxide/Graphene Oxide Composites Exploitable in Wastewater Treatments

Simona Ortelli [1,*], Lara Faccani [1], Enrico Ercolani [1,2], Ilaria Zanoni [1], Chiara Artusi [1], Magda Blosi [1], Stefania Albonetti [2] and Anna Luisa Costa [1]

[1] CNR-ISSMC, National Research Council of Italy-Institute of Science, Technology and Sustainability for Ceramics, Via Granarolo 64, 48018 Faenza, Italy; lara.faccani@me.com (L.F.); enrico.ercolani97@gmail.com (E.E.); ilaria.zanoni@issmc.cnr.it (I.Z.); chiara.artusi@issmc.cnr.it (C.A.); magda.blosi@issmc.cnr.it (M.B.); anna.costa@issmc.cnr.it (A.L.C.)

[2] Department of Industrial Chemistry "Toso Montanari", Bologna University, Viale Risorgimento 4, 40136 Bologna, Italy; stefania.albonetti@unibo.it

* Correspondence: simona.ortelli@issmc.cnr.it

Abstract: Water is one of the necessities for human survival, and clean water is essential for life. As a result, there is an increasing focus on efficient wastewater treatment methods, including advanced oxidation processes using innovative heterogeneous photocatalysts. In this context, TiO_2–graphene oxide (TGO) composites offer a multifaceted approach to wastewater treatment, combining the photocatalytic properties of TiO_2 with the adsorption capabilities and potential synergistic effects of graphene oxide. In this research, we intimately mixed commercial TiO_2 powder with graphene oxide at different concentrations (9, 16, and 25 wt.%) by exploiting sonochemical activation. The morphological and physicochemical analyses confirmed the interfacial interactions and the successful formation of the composite. The TGO composites exhibited increased reactivity compared to both GO and TiO_2 phases, during the photodegradation process of Rhodamine B (RhB), serving as a reaction model. Therefore, the photocatalytic results demonstrated the synergistic effect that occurs when a TiO_2-based photocatalyst is combined with sonochemically activated GO. The Cu^{2+} adsorption tests, simulating the removal of heavy metals from contaminated water, revealed that TGO composites displayed intermediate capabilities compared to the pure phases' higher (GO) and lower (TiO_2) adsorption capacity. The functional characterizations revealed that the optimal design is represented by the sample containing 16 wt.% of GO. Overall, this study confirms that TGO composites are effective as photocatalysts and adsorbents for removing both organic and inorganic pollutants, making them strong candidates for wastewater treatment.

Keywords: titanium dioxide/graphene oxide composites; photocatalysis; adsorption capacity

Academic Editors: Monica Brienza and Laura Scrano

Received: 9 May 2025
Revised: 12 June 2025
Accepted: 14 June 2025
Published: 17 June 2025

Citation: Ortelli, S.; Faccani, L.; Ercolani, E.; Zanoni, I.; Artusi, C.; Blosi, M.; Albonetti, S.; Costa, A.L. Design and Properties of Titanium Dioxide/Graphene Oxide Composites Exploitable in Wastewater Treatments. *Water* **2025**, *17*, 1809. https://doi.org/10.3390/w17121809

1. Introduction

Water is one of the necessities for human survival. Clean water is essential for life, and guaranteeing access to water and sanitation, along with their sustainable management, was established as one of the 17 Sustainable Development Goals (SDGs) that world leaders committed to achieving by 2030 to create a better future [1–3]. The water quality of aquatic environments is deteriorating, and this is attributed to pollutants such as dyes, metals, persistent organic pollutants (POPs), etc. [4]. Additionally, there are new generation pollutants, i.e., Emerging Contaminants (ECs), including Pharmaceuticals and Personal Care Products (PPCPs) [5], antimicrobial ingredients, hormonal compounds, plastic particulates, and

washing agents [6], derived from different sources, i.e., effluent discharges from wastewater treatment plants, industrial wastewater, agricultural practices, and urban rainwater runoff. There has been a growing emphasis on exploiting heterogeneous photocatalysts in advanced oxidation processes (AOPs) [7]. Currently, numerous semiconductors have been explored, with TiO_2 being the most extensively investigated, alongside its various doped or composite variants [8–12]. The research focused on doping TiO_2 with metals, coupling with a further semiconductor, or hybridizing TiO_2 with mesoporous, zeolite, or carbon-based frameworks, to improve the interaction with target pollutants and the photodegradation efficiency of the catalysts [13]. Integrated treatment systems that combine multiple remediation techniques, such as nano-mediated AOPs with membrane filtration, nanoadsorption, or bioremediation, can provide enhanced removal efficiency for a broad spectrum of ECs [14]. The design strategies aim to maximize the photocatalytic activity of the composite materials, improving the adsorption ability, slowing down the charge carrier's recombination, and optimizing light utilization [15,16]. Between the carbon-based material, graphene oxide (GO), the oxygenated byproduct of graphene, exhibits fascinating chemical, optical, and electrical properties, making it a highly promising candidate for addressing water pollution challenges. Its extensive surface area, along with oxygen-rich functional groups on its surface, enhances its affinity towards various pollutants, including heavy metals, organic compounds, and dyes [17,18]. Incorporating graphene oxide (GO) into the design of TiO_2-based photocatalysts for wastewater treatment can enhance their performance by improving their photocatalytic activity, stability, and reusability. The high porosity coupled with the efficient charge transport capability of GO can contribute to efficient electron-hole separation and the transfer of photogenerated charge carriers. The GO hydrophilicity and amphiphilicity can facilitate the dispersion of TiO_2 nanoparticles in aqueous solutions and promote the adsorption of organic contaminants onto the photocatalyst surface. Finally, GO can act as a sensitizer, effectively harvesting a broader light spectrum and transferring electrons to TiO_2 nanoparticles, thereby improving the overall photocatalytic efficiency [19–24]. TiO_2–graphene-based nanocomposites possess outstanding chemical, mechanical, and electrical properties, making them promising materials for wastewater treatment through adsorption, filtration, and photodegradation. However, challenges remain in understanding their photocatalytic mechanisms, particularly under visible light, and improving their stability, reusability, and scalability. Surface modifications and hybrid designs are being explored to enhance charge separation, reduce agglomeration, and improve performance in real-world conditions. Despite their potential, cost-effective, large-scale production methods are needed to make these materials more practical for widespread environmental applications [25,26]. Recently, N. Naghavi and colleagues [27] developed TiO_2–graphene nanocomposites using a facile and cost-effective hydrothermal method with supercapacitive properties. The preparation of TiO_2-decorated GO nanosheets using the impregnation method was described by B. Bhattacharyya et al. [27]. According to the authors, the nanocomposite was specifically designed to maximize its catalytic efficiency in degrading neutral common and resilient industrial pollutants. Then, A. Basso Peressut and colleagues developed composite self-assembling membranes obtained by the combination of reduced graphene oxide (rGO) with titanium dioxide (TiO_2) able to capability to treat wastewater containing both inorganic and organic pollutants by exploiting the established ability of rGO to capture metal ions together with that of TiO_2 to degrade organic substances [28]. In this work, we exploited a user-friendly and adaptable-to-larger-scales method to blend commercial TiO_2 powder with different concentrations of graphene oxide by sonochemical activation. Sonication helps break down the graphite layers into individual GO sheets, facilitating their dispersion in the solution and the interaction with the TiO_2 phase, generating improved attributes in the resulting material [29]. The TiO_2 and

GO-based composite are promising for water treatment technology due to GO's proven effectiveness in removing inorganic pollutants and titanium dioxide's well-documented ability to break down organic contaminants. The goal is to integrate the capacity to both capture metal ions and photodegrade organic pollutants [30–33]. We then tested the photocatalytic properties, oxidative potential, and adsorption capacity of the resulting composites, comparing their reactivity with that of the individual components to explore the possibility of synergistic effects and determine the optimal composite composition.

2. Materials and Methods

2.1. Materials

TiO_2 powder DT-51 was supplied by CristalACTiV™ (Thann, Colmar, France). Graphite powder was purchased from Magaldi Power S.p.A. (Salerno, Italy). Rhodamine B (dye content ≈ 95%) used as target dye, hydrogen peroxide—H_2O_2 (30%), hydrochloric acid—HCl (37%), sodium nitrate—$NaNO_3$ (>99%), potassium permanganate—$KMnO_4$ (99.5%), and absolute ethanol (>99.8%) were provided by Sigma-Aldrich (Milan, Italy). Sulfuric acid—H_2SO_4 (96%) was purchased from Titolchimica (Rovigo, Italy).

2.2. Synthesis of TGO

The graphene oxide used was synthesized from graphite powder using the modified Hummer method [34]. Next, 2 g of $NaNO_3$ and 25 mL of concentrated H_2SO_4 were added to a synthesis flask when the sodium nitrate was completely dissolved, and 2 g of graphite powder was added for exfoliation. Then, mechanical mixing was performed for 2 h while maintaining the temperature using ice. Making sure that the temperature was <20 °C, 4 g of $KMnO_4$ was slowly added and left under mechanical stirring for 24 h, and a color change of the mixture from black to dark green was noted. After 24 h, while maintaining mechanical stirring, 100 mL of deionized H_2O was added. In this phase, a violent increase in temperature occurred with a consequent brown gas emission. Then, the temperature was kept constant at 98 °C for 15 min. Then, 200 mL of hot deionized water was added. When the temperature dropped below 60 °C, H_2O_2 (30 mL–30%) was added to eliminate $KMnO_4$ residues. Gold-colored bubbles were observed on the surface. The obtained sample was washed three times with HCl (10%) and once with deionized water to eliminate the residues of H_2SO_4. Finally, the suspension was dried in a vacuum oven at 80 °C for 15 h to obtain the GO sheets. After, the powder was hand-ground and sieved (mesh 80 μm).

TGO composite was obtained by mixing 0.5 g TiO_2 DT-51 nanopowder with different weight percentages of GO compared to TiO_2 (9, 16, and 25%) through sonochemical activation; the obtained samples were called TGO_9%, TGO_16%, and TGO_25%, respectively. Specifically, TiO_2 DT-51 powder was dispersed in 20 mL of absolute ethanol, and then a different amount of graphene oxide was added. The composite was subjected to 1 h of ultrasound probe (Bandelin sonoplus), maintaining an ice bath that prevents overheating of the suspension. The suspension was dried in an oven at 120 °C until complete evaporation of the solvent [35].

2.3. Physicochemical Characterization

Oxidation degree of GO through Fourier transform infrared spectroscopy—Attenuated total reflectance (FTIRATR) analysis

The FTIR analysis was carried out using the Nicolet iS5 instrument (Thermo Fischer, Milan, Italy). The measurement was performed in ATR mode, and the acquired spectral range was 415–3920 cm^{-1}; the spectral resolution used was 0.1 cm^{-1}. The oxidation degree of synthetized GO using the modified Hummer method was determined by quantitative analysis of the FTIR spectra.

X-ray diffraction (XRD)

The XRD measurements were conducted at room temperature with a Bruker D8 Advance X-ray diffractometer equipped with a fast X'Celerator detector (Bruker, Billerica, MA, USA), using a Cu anode as the X-ray source (Kα, λ = 1.5418 Å). Diffractograms were recorded in the range 5–80° 2θ counting for 0.2 s every 0.05° 2θ step.

Field emission scanning electron microscopy (FESEM)

GO and TGO composite (TGO_16%) powders were morphologically characterized by scanning electronic microscopy analysis using a Zeiss Sigma NTS microscope (Zeiss, Öberkochen, Germany). The powder samples were fixed to aluminum stubs with conductive adhesive tape and sputter-metalized with gold.

Transmission electron microscopy (TEM)

The transmission electron analyses were performed using a FEI TECNAI F20 microscope (FEI, Hillsboro, OR, USA) operating at an acceleration voltage of 200 keV. The powders (GO and TGO_16%) were dispensed in ultrapure water, and one drop of suspensions was deposited on a film-coated copper grid and then dried at 80 °C.

Specific surface area

The specific surface area was measured by N_2 physisorption apparatus (Surfer Thermo Scientific, Waltham, MA, USA) via Brunauer–Emmett–Teller (BET) analysis on TiO_2 DT-51, GO, and TGO composites.

Band gap energy measurements

The measurement of band gap energy of semiconductor materials involves the use of optical spectroscopy in diffuse reflectance using a LAMBDA 750 UV/VIS/NIR spectrophotometer (Perkin Elmer, Waltham, MA, USA) equipped with a 150 mm integrating sphere. The value of diffuse reflectance (%R), obtained by spectrophotometric measurements, can be converted into a value that is proportional to the absorption coefficient of the material F(R) by the equation of Kubelka–Munk (1):

$$F(R) = \frac{(1-R)^2}{2R} \quad (1)$$

To determine band gap energy, the graphical method was performed. It is a good method because it considers the nature of the electronic transitions that occur within the material. Then, the equation of Tauc (2) is applied:

$$\alpha h\nu = A\left(h\nu - E_g\right)^n \quad (2)$$

where α is the absorption coefficient of the material (which is proportional to F(R)), h is Planck's constant, ν is the frequency of the incident radiation, A is a constant, and the coefficient n indicates the electronic transition; in this case, $n = 2$. Finally, to determine the correct value E_g, it is necessary to extrapolate the linear portion of the curve y = 0, from Tauc's graph, which correlates (F (R) $h\nu$) $1/n$ versus $h\nu$ [36].

2.4. Functional Characterization

Photodegradation test

The photocatalytic tests were carried out using the photodegradation of Rhodamine B (RhB) as a reaction model; its molecular structure is shown in Figure S1a. RhB is a synthetic dye widely utilized as an organic trace pollutant due to the easy detection at low concentrations by spectrophotometric analysis using a single beam spectrophotometer Hach Lange, DR3900 (Hach, Loveland, CO, USA). RhB, when dissolved in water, imparts an intense magenta color and demonstrates a specific absorbance maximum at 554 nm (Figure S1a). The RhB photodegradation tests were conducted in a beaker at room temperature; the typical setup foresees the addition of photocatalysts, at 0.1 g L^{-1} concentration, to 150 mL of a

RhB aqueous solution. A dark equilibration period of approximately 60 min was employed to facilitate adsorption/desorption equilibrium between RhB and the catalyst, which was confirmed to be optimal for system stabilization. The suspension was stirred and irradiated by a UV lamp (OSRAM ultra-vitalux 300 W, UV-A 60 W/m^2, OSRAM, Munich, Germany) and solar simulator (SUN 2000 11000 model, Abet Technologies, Milford, CT, USA, 1000 W intensity). The emission spectra of UV light and solar simulator are reported in Figure S2. To stabilize the light output, the lamps were activated before initiating the photocatalytic experiments. The measurements were conducted using a quartz cuvette as sample holder. At 15, 30, 60, 90, and 120 min, 3 mL of the reaction mixture was withdrawn, and centrifuged (7500 rpm, 10 min), and the absorbance was measured at 554 nm to monitor degradation progress. The photocatalytic activity was quantified as the photodegradation rate constant of the catalyst, k (min^{-1}). The photodegradation of RhB in the presence of a catalyst can be considered a pseudo-first-order reaction and can be described by Equation (3):

$$ln\left(\frac{A_0}{A_x}\right) = k * t \quad (3)$$

As described by the Lambert–Beer law, absorbance is proportional to dye concentration. Therefore, ln (C_0/C) is determined using absorbance values measured initially (A_0) and after a certain irradiation interval (A_x). The apparent rate constant k was obtained through linear regression of ln(C_0/C) versus time. The conversion, calculated at t = 120 min, indicates the ratio between the amount of reagent consumed and the amount of reagent initially present in the reaction environment, and it is determined by Formula (4):

$$\text{Conversion}(\%) = \left(1 - \frac{A_x}{A_0}\right) * 100 \quad (4)$$

The photocatalytic results were obtained by averaging three measurements. A great reproducibility was obtained, considering the data of the three replicas, under both UV and solar light, as evidenced by the corresponding standard deviation values (Figure S3 and Figure S4, respectively).

Oxidative potential tests

The oxidative potential tests were performed on powder samples. The generation of specific hydroxyl ($^{\bullet}OH$) radicals was evaluated using a probe molecule: p-nitrosodimethylaniline (RNO). The oxidation of RNO can be followed spectrophotometrically: the degree of discoloration of RNO provides a measure of the tendency of the target materials to produce $^{\bullet}OH$. The aqueous solution of RNO appears yellow. When the RNO reacts with hydroxyl radical, the N=O double bond is destabilized with the consequent formation of the N-OH bond and the loss of the yellow color (Figure S1b). The powders were dispersed in 5 mL of PBS 0.01 M at 50 mg/L. The suspension was ultrasonicated for 5 min, and then 0.2 mL of RNO 40 μM were added to the suspension. The samples were left in the dark condition at 25 °C for 1 h and 4 h. The dark condition was compared to the UV light irradiation condition, where the samples were put under a UV lamp (OSRAM ultra—vitalux 300 W lamp—irradiance of UV-A: 60 W/m^2) for 1 h and 4 h. After the incubation time, the samples were centrifuged (4500 rpm for 8 min) to separate powders from the solution. The absorbance of RNO was assessed by spectrophotometer Hach Lange, DR3900. For each exposure time, three replicates were analyzed, and the results were reported as averages of these three independent measurements of absorbance.

Adsorption tests

The samples, in powder, were dispersed in water and brought into contact with a $CuCl_2$ solution (10 mg L^{-1}) at room temperature in a pH range of 4.5 to 5.5. The tests were conducted under stirring conditions, using 1 g L^{-1} of each sample (TiO_2 DT-51, GO, and TGO composites). To assess the sorption capacity, after exposure to Cu^{2+}, 8 mL of the solution was centrifuged at 4500 rpm for 40 min using centrifugal filter units (Polyethersulfone, 5 kDa, Amicon, Merck Millipore, Milan, Italy). This step allowed the separation of the solid phase from the liquid, enabling the quantification of unabsorbed Cu^{2+} in the solution over time intervals (1, 5, 15, 45, 60 min, and 24 h) by Inductively Coupled Plasma Optical Emission Spectroscopy (ICP-OES 5100, vertical dual view, Agilent Technologies, Santa Clara, CA, USA) equipped with a OneNeb nebulizer. Analyses were performed in radial view mode. Calibration curves were prepared using standards at 0.1, 1.0, 10.0, and 100.0 mg L^{-1}, with nitric acid added to both standards and diluted samples (1:10 *v*/*v*). The calibration curves showed good linearity, with correlation coefficients (R^2) exceeding 0.99. The results, expressed in mg Cu^{2+}/g_{sample}, were calculated from ICP-OES data averaged from three independent measurements.

3. Results and Discussion

3.1. Physicochemical Characterization

The GO FTIR spectrum (Figure 1) indicates the typical oxygen-rich groups expected on the surface of oxidized graphene. At higher wavenumbers than 2000 cm^{-1}, there are OH/H_2O bands corresponding to intercalated water; at 1020 and 1040 cm^{-1}, bands corresponding to the epoxy (C-O-C) stretching mode; at 1244 cm^{-1}, bands corresponding to bending mode of hydroxyl groups (C-OH); at 1726 cm^{-1}, bands corresponding to carbonyl functional groups located on the edge of the graphene oxide sheets (yet not COOH and C=O); finally, at 1570 cm^{-1}, bands corresponding to the C=C vibration of the graphene skeleton [37]. For comparison analysis, the TiO_2 DT-51 and TGO_16% spectra are also reported in Figure 1. In the TiO_2 DT-51 spectrum, a broad band in the wavenumber range 900–400 cm^{-1} and the peak at 1630 cm^{-1} is assigned to the Ti-O-Ti and Ti-OH stretching modes, respectively. Asymmetrical and symmetrical stretching vibrations of the hydroxyl group can be observed at 3400 cm^{-1}. In the TGO composite spectrum, it is possible to detect the main peak of TiO_2 and GO phases. In addition, the shift of the broad band in the 900–400 cm^{-1} region toward lower wavenumbers may indicate the presence of Ti-O-Ti and Ti–O–C bonds within the composite, suggesting a chemical interaction between the surface hydroxyl groups of TiO_2 and the functional groups present on GO [38,39]. The oxidation degree (OD) of synthesized GO using the modified Hummer method was determined by semi-quantitatively assessing the FTIR spectra. Specifically, a linear baseline was subtracted from raw spectra. The resulting spectra were multiplied by −1 to obtain positive bands and the origin at y = 0. First, the total area (A_{tot}) from the original spectra was calculated. Then, the area corresponding to the aromatic C=C peak ($A_{C=C}$) at 1570 cm^{-1} (considering the wavenumber range from 1525 to 1625 cm^{-1}) was calculated. To measure these areas, the Simpson method was used. Finally, the OD of the graphene oxide was determined through Equation (5) as a ratio of the sum of all oxygen bands (A_{tot}) subtracting the aromatic band ($A_{C=C}$) from the total spectrum to the total area.

$$OD = \frac{A_{tot} - A_{C=C}}{A_{tot}} \quad (5)$$

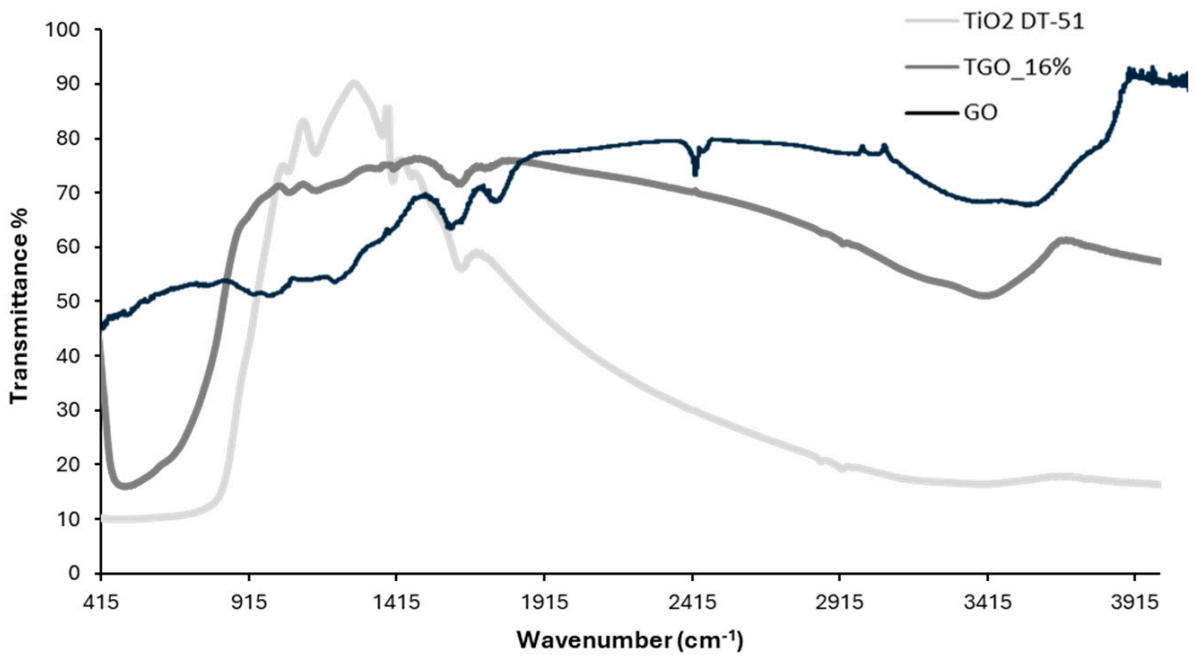

Figure 1. FTIR spectra of TiO_2 DT−51, TGO_16%, and GO sample.

The OD resulted around 1 (in the specific 0.998), demonstrating a complete oxidation of graphene in GO as also shown by the XRD analysis (Figure S6).

The FESEM image of GO (Figure 2a) reveals thin, irregularly stacked sheets in close proximity, resulting in a structurally disordered solid. TEM image (Figure 2b) clearly shows the flakes of GO demonstrating that exfoliation has effectively occurred. The HRTEM image (Figure S5a) depicts sheet stacks confirming a multilayer structure. The diffractogram of the GO sample (Figure S6) displays a prominent diffraction peak near 12°, attributed to the (002) plane of GO, along with a second peak around 43°, corresponding to the (100) plane. FESEM and TEM images of TGO composites (Figure 2c,d) showed a clumped distribution of TiO_2 nanoparticles (NPs) on the surface of the GO sheets confirmed also by the HRTEM image (Figure S5b). We can assume that a self-assembled coating of TiO_2 particles is deposited on GO sheets during the sonochemical process. In summary, the morphological characterization reveals a strong interaction between the TiO_2 nanoparticles and GO sheets. This good interfacial adhesion suggests a favorable synergy, essential for enhancing the photocatalytic performance of the composite [40]. The specific surface area data, presented in Table S1, confirm that the surface area of GO increases significantly in the composite due to the presence of well-dispersed TiO_2 nanoparticles. As demonstrated by the literature data, the composite TiO_2–GO showed a more enhanced surface area than pure TiO_2 [41,42]. Moreover, the introduction of GO significantly increases the total pore volume, with values reaching up to 16.3 cm^3/g in the rGO–TiO_2 composites [43]. Figure 3 presents the X-ray diffractograms of TiO_2 compared with TGO composites. TiO_2 DT-51 is composed only of the anatase phase in agreement with the information reported on the commercial data sheet [44]. The TGO composite showed the presence of both phases, anatase and graphene oxide. Increasing the amount of GO in TGO samples, we observed a corresponding slight increase in diffraction peak around 12°, assigned to the (002) plane of GO (see the inset in Figure 3).

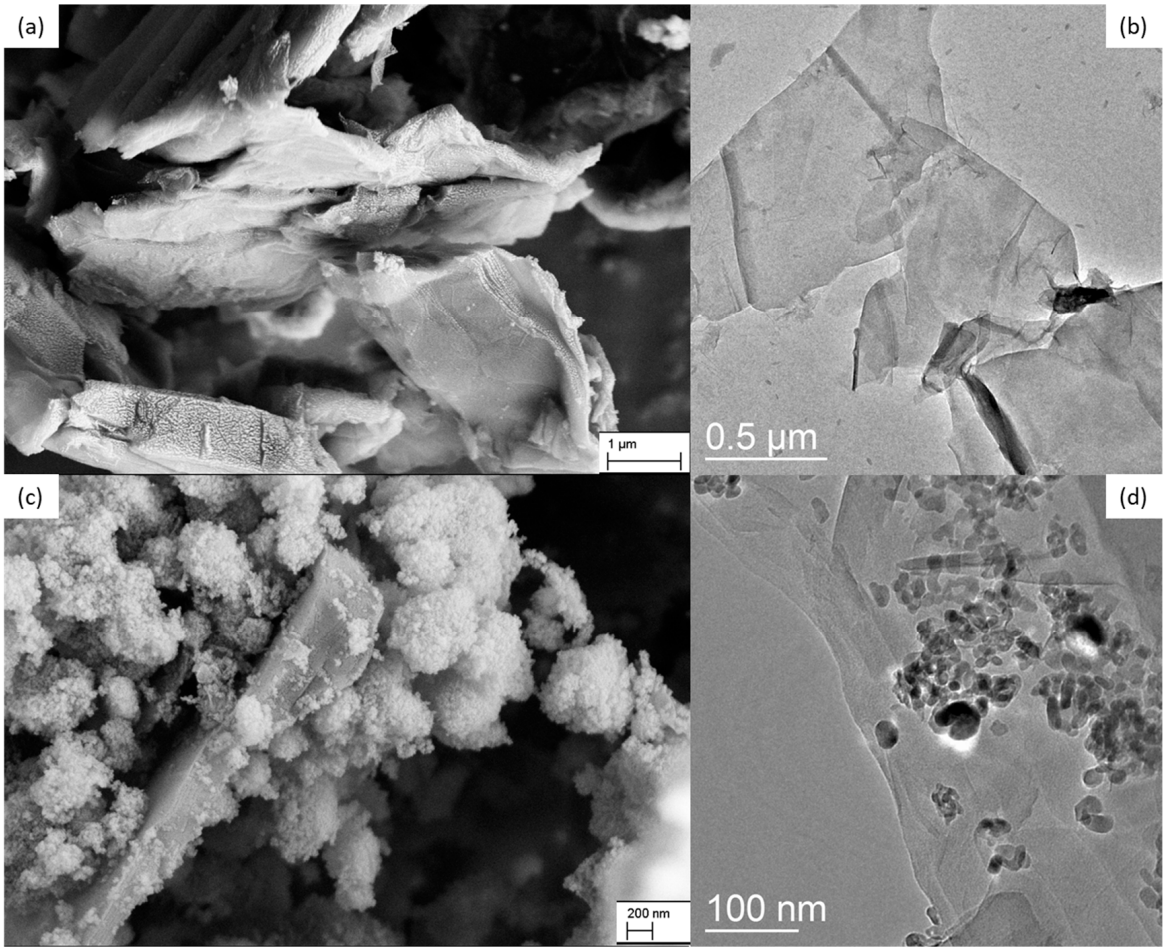

Figure 2. (**a**) FESEM and (**b**) TEM image of GO sample; (**c**) FESEM and (**d**) TEM image of TGO_16% sample.

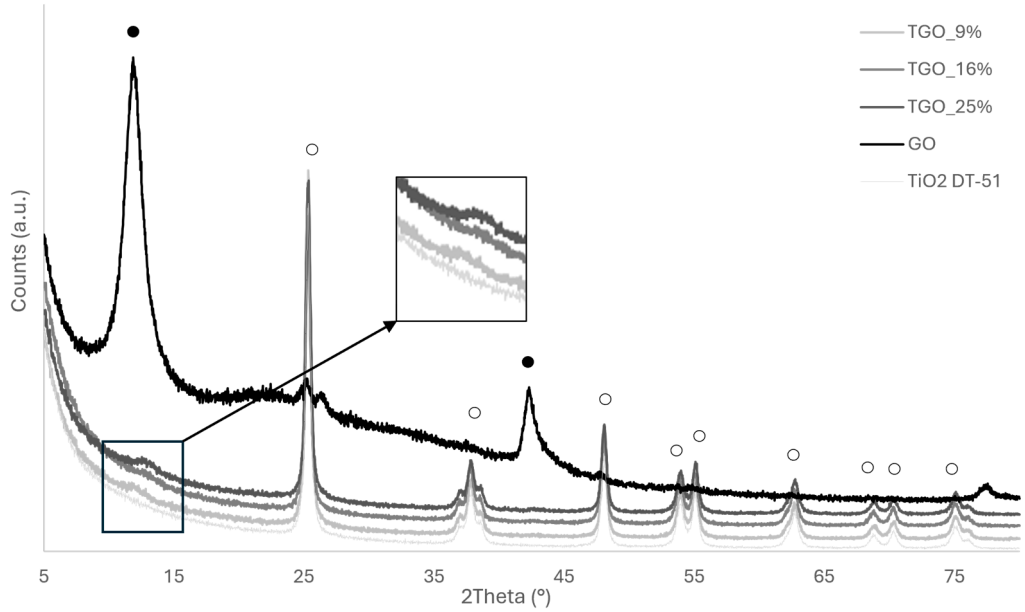

Figure 3. XRD patterns for TiO_2 DT-51; GO; TGO_9%; TGO_16%; and TGO_25%; ○ = anatase; ● = graphene oxide. The inset shows a zoom of the region in correspondence with the diffraction peak attributable to the (002) plane of GO.

3.2. Functional Characterization

The photocatalytic tests performed under UV light without catalysts did not show any color change, confirming that the RhB degradation did not occur by photolysis (pink curve in Figure 4a). The degradation of RhB with the pure anatase (TiO_2 DT-51) or GO phases, as photocatalysts, resulted in nearly 64% and 47% degradation of the dye, after 120 min, respectively, with a kinetic constant (K) equal to 8.3×10^{-3} min^{-1} and 5.3×10^{-3} min^{-1} (Table 1). The degradation efficiency of the individual components significantly improved in the TGO composites (Figure 4a), indicating a synergistic effect resulting from the combination of TiO_2 and GO phases. This improvement is attributed to GO, which promotes the adsorption of target molecules that diffuse to the phase boundary or the interphase facilitating the interaction with photoinduced oxidative radicals. In addition, GO behaves as electron scavengers boosting the electron transfer rate of TiO_2 and inhibits charge carrier recombination [38,45–47]. The sample TGO_16% showed the highest efficiency with almost 80% dye degradation and a kinetic constant $k = 1.4 \times 10^{-2}$ min^{-1}. At a higher GO content, the performance decreased, likely due to an excess of GO masking or competing with the active sites of TiO_2.

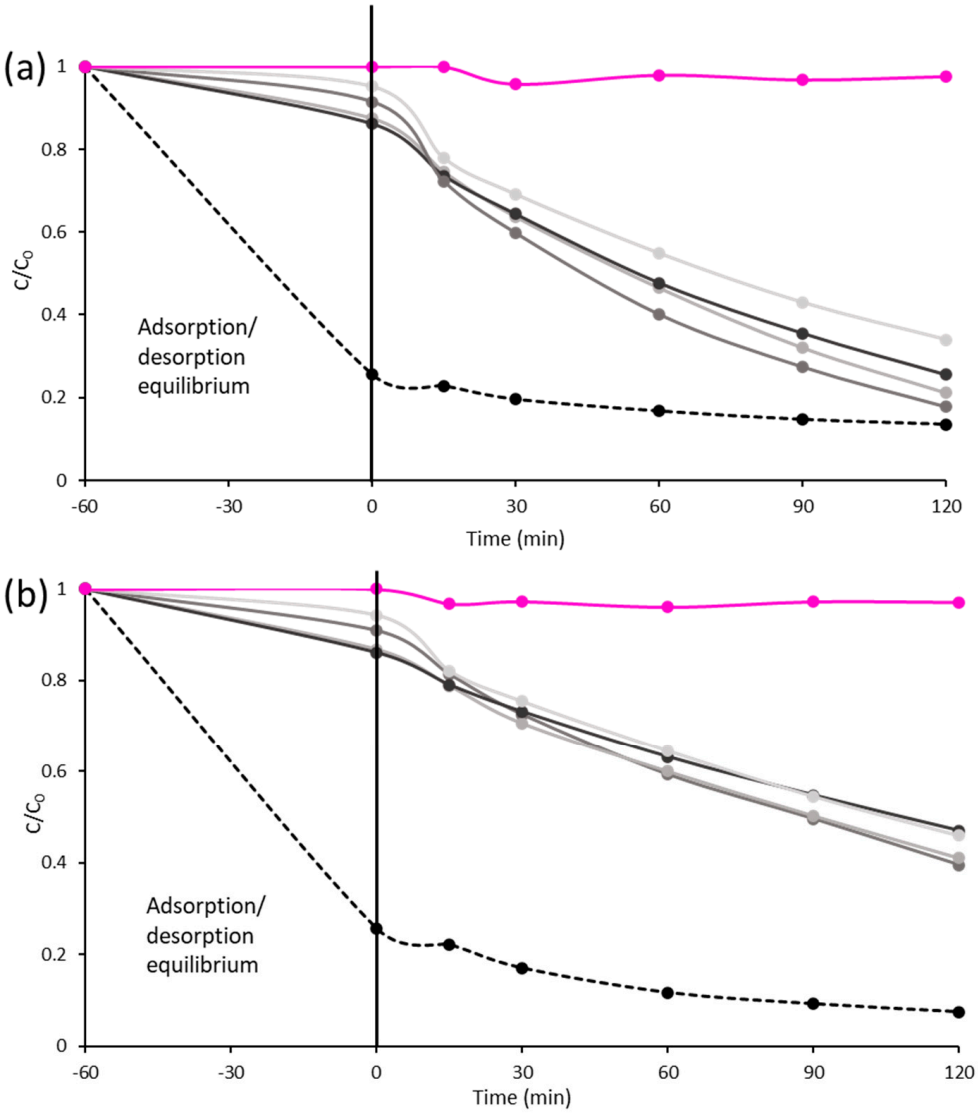

Figure 4. Dye degradation comparing different photocatalysts: • without photocatalyst (no degradation occurred by photolysis); • TiO_2 DT−51; • TGO_9%; • TGO_16%; •TGO_25%; • GO (dashed curve), under (**a**) UV light and (**b**) solar light.

Table 1. Band gap (Eg) and kinetic constants (k) from photocatalytic tests under both UV and solar light.

Sample	E_g (eV)	UV Light	Solar Light
		k (min^{-1})	k (min^{-1})
TiO_2 DT-51	3.25	8.3×10^{-3}	5.8×10^{-3}
GO	nd *	5.3×10^{-3}	nd *
TGO_9%	3.22	1.2×10^{-2}	6.2×10^{-3}
TGO_16%	3.21	1.4×10^{-2}	6.8×10^{-3}
TGO_25%	3.18	1.0×10^{-2}	5.0×10^{-3}

Note: * not determined.

The same tests were performed under solar light (Figure 4b). The photodegradation of RhB with the pure anatase (TiO_2 DT-51) resulted in a nearly 50% degradation of the dye, after 120 min, with k = 5.8×10^{-3} min^{-1} (Table 1). The high adsorption of dye during the establishment of absorption/desorption equilibrium, when the samples were left in the dark for 1 h (see dashed curve before t = 0), prevented an estimation of the GO sample potential contribution once activated by light [48]. Also, in this case, the TGO composites presented an enhanced RhB conversion, with TGO_16% again being the best-performing sample with a RhB conversion of nearly 56% and k = 6.8×10^{-3} min^{-1}. To verify if the sonochemical activation used during the preparation of composites effectively contributed to the formation of the composite and its enhanced final reactivity, we compared the conversion % of RhB (under UV light), TiO_2, TGO_16%, and a simple blend of TiO_2 and GO. The data showed that the RhB conversion of TiO_2 and GO just mixed (TiO_2/GO) was equal to that of pure TiO_2 DT-51 (Table 2). This finding demonstrated that sonochemical activation is essential for establishing an effective interaction between the two phases and benefiting from the synergistic effect observed in the photodegradation tests [20,49].

Table 2. Conversion % after 120 min of RhB photodegradation tests, under UV light.

Sample	RhB Conversion %
TiO_2 DT-51	64 ± 3.3
TGO_16%	80 ± 4.9
TiO_2/GO	64 ± 4.2

Instead, there was no linear correlation between the RhB photodegradation activity and the specific surface area (Table S1) of the TGO composite varying the GO content.

Comparing the results under the two light sources, we found that the photocatalytic performance under UV light was higher than that under solar light in agreement with the band gap data of Table 1, showing similar E_g for both TiO_2 DT-51 and TGO composites, around the typical value of anatase (3.20 eV) [50,51]. In Figure S7, Tauc's graph is reported; from which, the band gap value is calculated for each sample. Moreover, this finding suggests that in our sample, GO does not function as a photosensitizer, which would be expected to enhance electron–hole separation efficiency and, consequently, photocatalytic activity. Instead, the observed improvement in RhB photodegradation under UV light can be attributed to the likely adsorption of target molecules by GO. These molecules then diffuse to the phase boundary or interphase, facilitating their interaction with photoinduced oxidative radicals [47]. To enhance performance under visible light, previous studies suggest using photocatalysts with metals [52–56]. However, many of these elements are high cost and environmentally damaging. Moreover, their inclusion in photocatalytic systems can result in photochemical degradation (photo-corrosion). Although total degradation was not achieved under solar light, we demonstrated that TGO is a valid photocatalyst

because of its low toxicity and good performance. We are aware that obtaining excellent photocatalytic properties, under UV light, remains a limitation in real applications [57].

A comparison study of the developed material based on TiO_2 and GO with the previous work is shown in Table 3. The data of RhB photodegradation confirmed that our TGO materials have functional performance and a % of GO in line with photocatalysts developed in previous works.

Table 3. The UV-induced photodegradation of RhB in this work in comparison with prior studies.

Photocatalyst Material	%GO	Synthesis Method	RhB Conversion %	Reference
TiO_2-rGO	6	Hydrothermal	97.9	[46]
N-TiO_2/rGO	nd *	Sonication	78.29	[58]
TiO_2-rGO	10	Hydrothermal	86.81	[59]
TiO_2GO	33.3	Microwave	82.9	[60]
TGO	16	Sonication	80.0	Present study

Note: * not determined.

The oxidative potential tests were performed on powder samples to evaluate the hydroxyl ($^{\bullet}$OH) radicals' production under UV light irradiation and dark conditions (Figure 5). The results, expressed as moles of RNO consumed on mg of photocatalyst in powder as a function of time, showed that RNO depletion of GO sample is not affected by light, meaning that the main consumption can be attributed to RNO adsorption and not on $^{\bullet}$OH production. On the other hand, the TiO_2-based materials showed a significant improvement in RNO consumption once exposed to light. TGO_16% was again the most promising composite, providing the highest consumption at 1 h, while after 4 h of exposure, the composites gave comparable results but still higher than the TiO_2 DT-51 sample alone. These findings confirm the synergistic effect that occurs when a TiO_2-based photocatalyst is combined with sonochemically activated GO, strengthening the interactions between TiO_2 and GO phases.

The results obtained by photocatalytic and oxidative potential tests allowed us to hypothesize the photodegradation mechanism. Light exposure initiates electron excitation in TGO from the valence band to the conduction band, creating electron–hole pairs. These charge carriers participate in redox reactions: electrons reduce O_2 to $^{\bullet}O_2^-$, and holes oxidize H_2O and OH^- to form $^{\bullet}$OH radicals, whose production was experimentally demonstrated by RNO consumption in the oxidative potential tests. Consequently, RhB molecules undergo oxidative degradation through reactions with $^{\bullet}O_2^-$ and $^{\bullet}$OH radicals, and, if the process is complete, they form CO_2 and H_2O as well as nitrogen composites. The hypothetical RhB photodegradation mechanism is reported in the Supplementary Materials.

Figure 6 and Table S2 (the data were expressed as % Cu^{2+} adsorbed with relative standard deviation) show the results of Cu^{2+} adsorption tests, aimed at simulating the removal of hazardous metals from contaminated water. The TGO composites exhibited intermediate adsorption capabilities, situated between the higher adsorption capacity of GO and the lower capacity of pure TiO_2. Moreover, we observed a negligible increase in Cu^{2+} adsorption as time progresses (except for GO), evidencing that the fast kinetic adsorption is observed in these samples. At longer times (24 h, Table S2), Cu^{2+} sorption decreased in all samples. This decrease could be justified by a desorption phenomenon, which is mainly attributed to GO sheet [61].

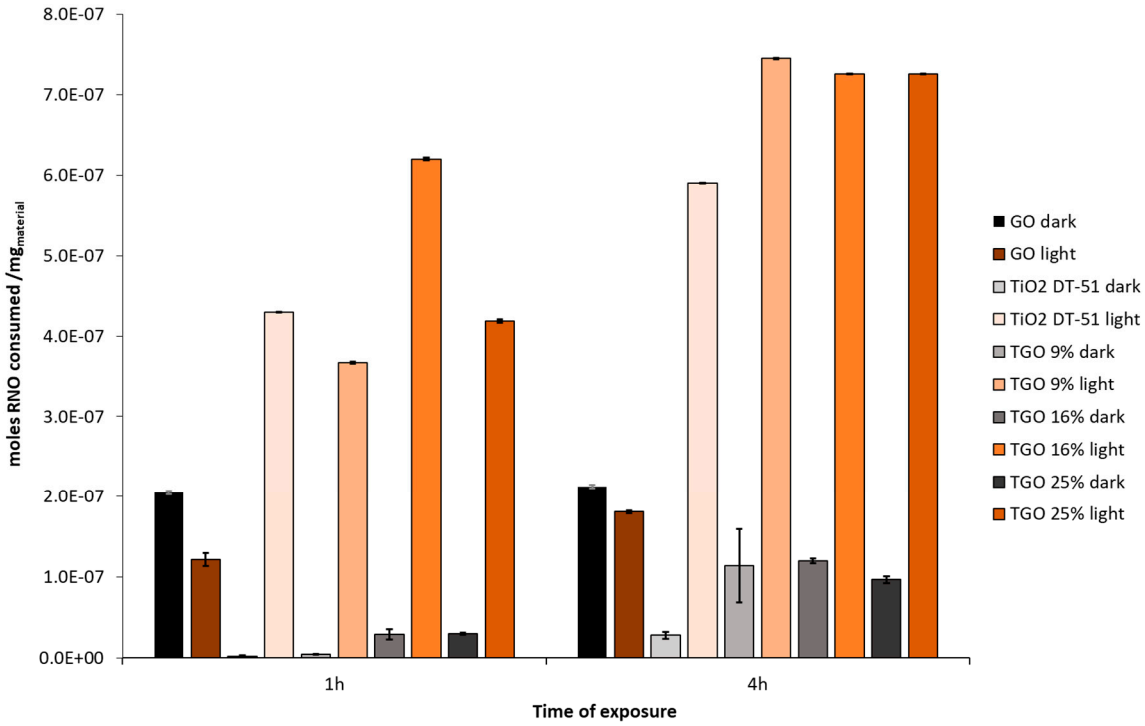

Figure 5. Oxidative potential of TiO_2, GO, and TGO composites under light and dark conditions, expressed as moles of RNO consumed on mg of phase dispersed.

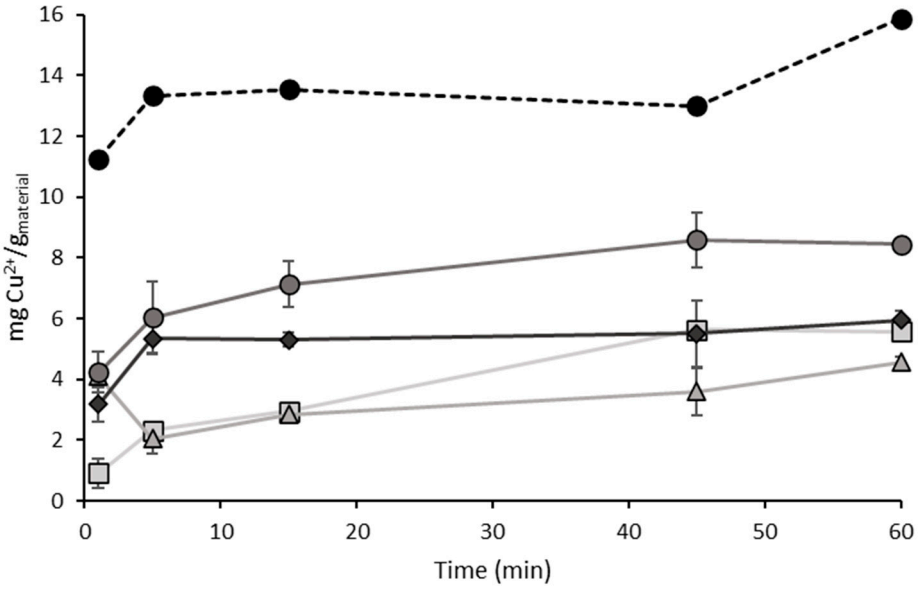

Figure 6. Sorption kinetics for □ TiO_2 DT-51; △ TGO_9%; ● TGO_16%; ◆ TGO_25%; • GO.

The highest adsorption observed in GO can be readily explained by considering the surface complexation ability of their functional groups (e.g., hydroxyl, epoxide, ketone, and carboxyl groups) that in TGO samples are partially masked by TiO_2 NPs deposited [62,63]. The adsorption activity of GO can occur through three main mechanisms: ion exchange, electrostatic attraction, and surface complexation [64]. However, upon comparing the data of TGO composites with the values calculated by the weighted average of GO and TiO_2 adsorption capacities (theoretical value), we observed a significant enhancement in the adsorption capacity of TGO_16% composite (Figure 7). This enhancement was not observed in the other composites (TGO_9% and TGO_25%), confirming TGO_16% is the optimal

design choice for the composite phase, as observed in Table S3, where it is highlighted that the functional properties improved up to the 16% GO content. The surplus GO is likely responsible for enveloping TiO_2 active sites and blocking incident light, thereby decreasing photocatalytic efficiency [65]. Moreover, the decrease in adsorption capacity in the TGO composite can be justified by the reduced availability of the functional groups of GO, which play a key role in adsorption, that are bound to the TiO_2 phase. As observed for the photocatalytic activity, there was no linear correlation between the adsorption capacity and specific surface area (Table S1) of the TGO composite varying the GO content. A comparison study of the adsorption capacity of the material based on TiO_2 and GO with the previous work [66–71] is shown in Table S4. The data showed that our TGO materials have an adsorption capacity slightly lower than the material developed in previous works. It is necessary to consider that the adsorption process was carried out under standard conditions without optimizing pH, temperatures, and the metal/adsorbent ratio. Moreover, our developed materials were produced starting from commercial TiO_2 whose main scope was improving its functional properties by adding GO. This has been successfully achieved by finding a synergistic effect, resulting from the combination of TiO_2 and GO, in the photocatalysis processes.

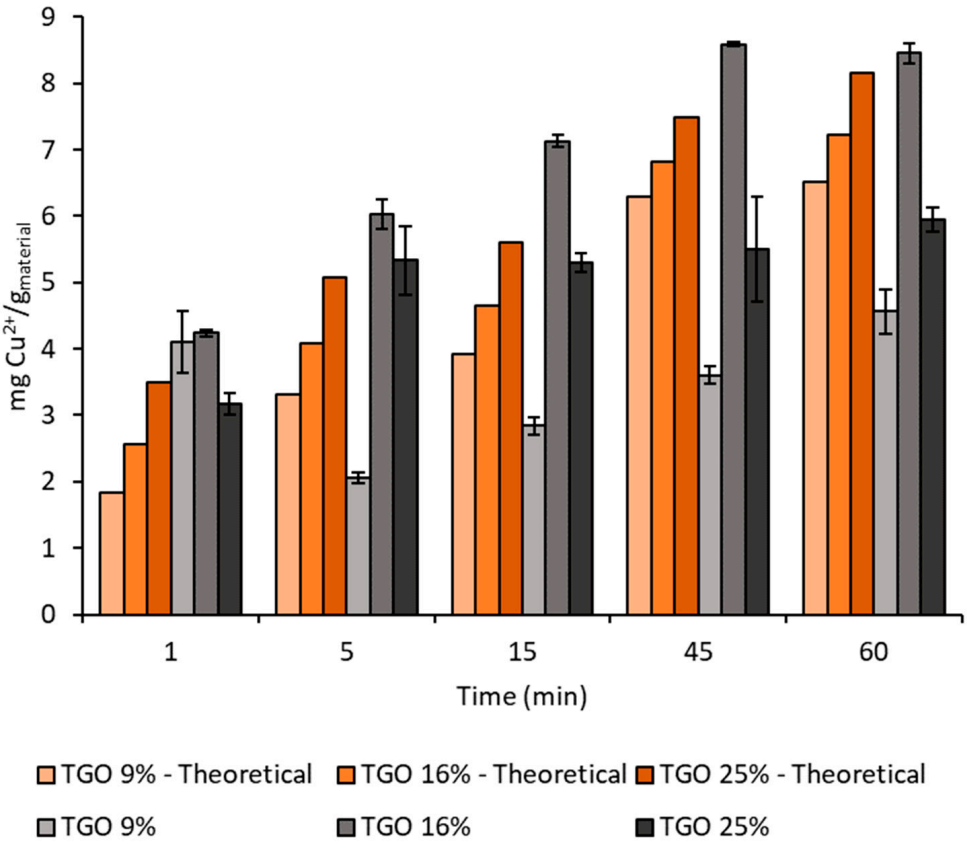

Figure 7. Cu^{2+} adsorption of TGO composites: comparison between theoretical (calculated) values by considering the weighted adsorption of the pure phases TiO_2/GO and experimental values.

4. Conclusions

Composite materials of titanium dioxide (TiO_2) and graphene oxide (GO) were prepared by a sonochemically activated mixture of commercial TiO_2 powder and graphene oxide, synthesized using the modified Hummers method. TGO samples with different GO content (9, 16, and 25%) were compared to identify the best design option. XRD and FTIR characterization analyses demonstrated that GO was successfully synthesized with a

calculated oxidation degree close to 1. Morphological analysis revealed sheet stacks with varying thicknesses, indicating that effective exfoliation has taken place. In TGO composites, strong interactions between TiO_2 nanoparticles and GO sheets were demonstrated. Two main functional properties were assessed. Photocatalytic tests, conducted under both UV and solar light, revealed the synergistic enhancement due to the integration of TiO_2 and GO, as confirmed by oxidative potential tests.

The Cu^{2+} adsorption tests, simulating the removal of heavy metals from wastewater, showed that TGO composites improved the adsorption capabilities compared to the two phases mixed without sonochemical activation. Both functional characterizations indicated that the optimal GO content in the TGO composite corresponded to 16%. In summary, TGO composites show promise as heterogeneous photocatalysts and adsorbents for effectively removing both organic and inorganic pollutants, positioning them as strong candidates for wastewater treatment. Considering the scalability and sustainability of the sonochemical method, future developments of TGO-based photocatalysts in real applications are possible without significant issues. However, a problem of real importance remains in the synthesis of GO, which has a strong negative environmental impact. Surely, the study of an eco-friendly synthesis must be a main objective for the use of TGO-based photocatalysts in real applications.

Supplementary Materials: The following supporting information can be downloaded at https://www.mdpi.com/article/10.3390/w17121809/s1. Figure S1: (a) Rhodamine B absorbance spectra; (b) oxidation reaction scheme of RNO; Figure S2: Emission spectrum of (a) UV lamp and (b) solar simulator; Figure S3: Photocatalytic degradation of RhB, under UV light, using as catalyst (a) TiO_2 DT-51; (b) TGO_9%; (c) TGO_16%; and (d) TGO_25%; Figure S4: Photocatalytic degradation of RhB, under solar light, using as catalyst (a) TiO_2 DT-51; (b) TGO_9%; (c) TGO_16%; and (d) TGO_25%; Figure S5: HRTEM images of (a) GO and (b) TGO_16% sample; Figure S6: XRD patterns for GO; Figure S7: Tauc's curve for TiO_2 DT-51 and TGO composites; Table S1: Specific surface area of TiO_2, GO, and TGO composites; Table S2: Results of Cu^{2+} adsorption (% Cu^{2+} adsorbed with relative standard deviation) tests; Table S3: Summary of photocatalytic (RhB conversion %, after 120 min, and moles of RNO consumed/mg of phase dispersed, after 1 h) and adsorption (% Cu^{2+} adsorbed, after 60 min) results; Table S4: The adsorption capacity in this study compared with previous studies; the hypothetical RhB photodegradation mechanism.

Author Contributions: Conceptualization: S.O., S.A. and A.L.C.; methodology: I.Z., E.E., L.F. and C.A.; investigation: I.Z., E.E., L.F. and C.A.; data curation: I.Z., E.E., L.F., C.A. and S.O.; writing—original draft preparation: S.O.; writing—review and editing: S.O., L.F. and A.L.C.; supervision: M.B., S.A. and A.L.C. All authors have read and agreed to the published version of the manuscript.

Funding: This research received no external funding.

Data Availability Statement: Data are provided within the manuscript and the Supplementary Information file.

Conflicts of Interest: The authors declare that they have no known competing financial interests or personal relationships that could have appeared to influence the work reported in this paper.

References

1. ONU. *Transforming Our World: The 2030 Agenda for Sustainable Development*; United Nations: New York, NY, USA, 2015.
2. UNICEF; WHO. Progress on Household Drinking Water, Sanitation and Hygiene 2000–2017: Special Focus on Inequalities. UNICEF: New York, NY, USA; Geneva, Switzerland, 2019; p. 140.
3. Frédéric, S. EU Commission Unveils 'European Green Deal': The Key Points. Available online: https://www.euractiv.com/ (accessed on 29 December 2019).

4. Clarke, R.M.; Cummins, E. Evaluation of "Classic" and Emerging Contaminants Resulting from the Application of Biosolids to Agricultural Lands: A Review. *Hum. Ecol. Risk Assess. Int. J.* **2015**, *21*, 492–513. [CrossRef]
5. Nikolaou, A. Pharmaceuticals and Related Compounds as Emerging Pollutants in Water: Analytical Aspects. *Glob. Nest J.* **2013**, *15*, 1–12. [CrossRef]
6. Azizi-Lalabadi, M.; Pirsaheb, M. Investigation of Steroid Hormone Residues in Fish: A Systematic Review. *Process Saf. Environ. Prot.* **2021**, *152*, 14–24. [CrossRef]
7. Kurian, M. Advanced Oxidation Processes and Nanomaterials—A Review. *Clean. Eng. Technol.* **2021**, *2*, 100090. [CrossRef]
8. Gatou, M.A.; Syrrakou, A.; Lagopati, N.; Pavlatou, E.A. Photocatalytic TiO_2-Based Nanostructures as a Promising Material for Diverse Environmental Applications: A Review. *Reactions* **2024**, *5*, 135–194. [CrossRef]
9. Zhang, S.; Gu, P.; Ma, R.; Luo, C.; Wen, T.; Zhao, G.; Cheng, W.; Wang, X. Recent Developments in Fabrication and Structure Regulation of Visible-Light-Driven g-C3N4-Based Photocatalysts towards Water Purification: A Critical Review. *Catal. Today* **2019**, *335*, 65–77. [CrossRef]
10. Devi, L.G.; Kavitha, R. A Review on Non Metal Ion Doped Titania for the Photocatalytic Degradation of Organic Pollutants under UV/Solar Light: Role of Photogenerated Charge Carrier Dynamics in Enhancing the Activity. *Appl. Catal. B Environ.* **2013**, *140–141*, 559–587. [CrossRef]
11. Acharya, R.; Parida, K. A Review on TiO_2/g-C_3N_4 Visible-Light-Responsive Photocatalysts for Sustainable Energy Generation and Environmental Remediation. *J. Environ. Chem. Eng.* **2020**, *8*, 103896. [CrossRef]
12. Mishra, S.; Marandi, B.; Sanjay, K.; Acharya, R. Graphitic Carbon Nitride Loaded $Bi_4O_5I_2$ for Elevated Photocatalytic Tetracycline Degradation. *Ournal Met. Mater. Miner.* **2025**, *35*, e2261. [CrossRef]
13. Xia, X.-H.; Jia, Z.-J.; Yu, Y.; Liang, Y.; Wang, Z.; Ma, L.-L. Preparation of Multi-Walled Carbon Nanotube Supported TiO2 and Its Photocatalytic Activity in the Reduction of CO_2 with H_2O. *Carbon N. Y.* **2007**, *45*, 717–721. [CrossRef]
14. Mofijur, M.; Hasan, M.M.; Ahmed, S.F.; Djavanroodi, F.; Fattah, I.M.R.; Silitonga, A.S.; Kalam, M.A.; Zhou, J.L.; Khan, T.M.Y. Advances in Identifying and Managing Emerging Contaminants in Aquatic Ecosystems: Analytical Approaches, Toxicity Assessment, Transformation Pathways, Environmental Fate, and Remediation Strategies. *Environ. Pollut.* **2024**, *341*, 122889. [CrossRef]
15. Chen, X.; Mao, S.S. Titanium Dioxide Nanomaterials: Synthesis, Properties, Modifications, and Applications. *Chem. Rev.* **2007**, *107*, 2891–2959. [CrossRef] [PubMed]
16. Burda, C.; Chen, X.; Narayanan, R.; El-Sayed, M.A. Chemistry and Properties of Nanocrystals of Different Shapes. *Chem. Rev.* **2005**, *105*, 1025–1102. [CrossRef]
17. Lerf, A.; He, H.; Forster, M.; Klinowski, J. Structure of Graphite Oxide Revisited. *J. Phys. Chem. B* **1998**, *102*, 4477–4482. [CrossRef]
18. Guerrero-Contreras, J.; Caballero-Briones, F. Graphene Oxide Powders with Different Oxidation Degree, Prepared by Synthesis Variations of the Hummers Method. *Mater. Chem. Phys.* **2015**, *153*, 209–220. [CrossRef]
19. Berberidou, C.; Kyzas, G.Z.; Paspaltsis, I.; Sklaviadis, T.; Poulios, I. Photocatalytic Disinfection and Purification of Water Employing Reduced Graphene Oxide/TiO_2 Composites. *J. Chem. Technol. Biotechnol.* **2019**, *94*, 3905–3914. [CrossRef]
20. Jiang, G.; Lin, Z.; Chen, C.; Zhu, L.; Chang, Q.; Wang, N.; Wei, W.; Tang, H. TiO_2 Nanoparticles Assembled on Graphene Oxide Nanosheets with High Photocatalytic Activity for Removal of Pollutants. *Carbon N. Y.* **2011**, *49*, 2693–2701. [CrossRef]
21. Saroyan, H.S.; Bele, S.; Giannakoudakis, D.A.; Samanidou, V.F.; Bandosz, T.J.; Deliyanni, E.A. Degradation of Endocrine Disruptor, Bisphenol-A, on an Mixed Oxidation State Manganese Oxide/Modified Graphite Oxide Composite: A Role of Carbonaceous Phase. *J. Colloid Interface Sci.* **2019**, *539*, 516–524. [CrossRef]
22. Trapalis, A.; Todorova, N.; Giannakopoulou, T.; Boukos, N.; Speliotis, T.; Dimotikali, D.; Yu, J. TiO_2/Graphene Composite Photocatalysts for NOx Removal: A Comparison of Surfactant-Stabilized Graphene and Reduced Graphene Oxide. *Appl. Catal. B Environ.* **2016**, *180*, 637–647. [CrossRef]
23. Zhang, H.; Wang, X.; Li, N.; Xia, J.; Meng, Q.; Ding, J.; Lu, J. Synthesis and Characterization of TiO_2/Graphene Oxide Nanocomposites for Photoreduction of Heavy Metal Ions in Reverse Osmosis Concentrate. *RSC Adv.* **2018**, *8*, 34241–34251. [CrossRef]
24. Giannakoudakis, D.A.; Farahmand, N.; Łomot, D.; Sobczak, K.; Bandosz, T.J.; Colmenares, J.C. Ultrasound-Activated TiO_2/GO-Based Bifunctional Photoreactive Adsorbents for Detoxification of Chemical Warfare Agent Surrogate Vapors. *Chem. Eng. J.* **2020**, *395*, 125099. [CrossRef]
25. Shaik, B.B.; Katari, N.K.; Raghupathi, J.K.; Jonnalagadda, S.B.; Rana, S. Titanium Dioxide/Graphene-Based Nanocomposites as Photocatalyst for Environmental Applications: A Review. *ChemistrySelect* **2024**, *9*, e202403521. [CrossRef]
26. Badoni, A.; Thakur, S.; Vijayan, N.; Swart, H.C.; Bechelany, M.; Chen, Z.; Sun, S.; Cai, Q.; Chen, Y.; Prakash, J. Recent Progress in Understanding the Role of Graphene Oxide, TiO_2 and Graphene Oxide-TiO_2 Nanocomposites as Multidisciplinary Photocatalysts in Energy and Environmental Applications. *Catal. Sci. Technol.* **2025**, *15*, 1702–1770. [CrossRef]
27. Naghavi, N.; Jalaly, M.; Mohammadi, S.; Mousavi-Khoshdel, S.M. An Investigation into the Influence of Graphene Content on Achieving a High-Performance TiO_2-Graphene Nanocomposite Supercapacitor. *ChemistryOpen* **2024**, *13*, 202400128. [CrossRef]

28. Basso Peressut, A.; Cristiani, C.; Dotelli, G.; Dotti, A.; Latorrata, S.; Bahamonde, A.; Gascó, A.; Hermosilla, D.; Balzarotti, R. Reduced Graphene Oxide/Waste-Derived TiO_2 Composite Membranes: Preliminary Study of a New Material for Hybrid Wastewater Treatment. *Nanomaterials* **2023**, *13*, 1043. [CrossRef]
29. Morales-Torres, S.; Pastrana-Martínez, L.M.; Figueiredo, J.L.; Faria, J.L.; Silva, A.M.T. Design of Graphene-Based TiO2 Photocatalysts—A Review. *Environ. Sci. Pollut. Res.* **2012**, *19*, 3676–3687. [CrossRef]
30. Mishra, S.; Acharya, R.; Parida, K. Spinel-Ferrite-Decorated Graphene-Based Nanocomposites for Enhanced Photocatalytic Detoxification of Organic Dyes in Aqueous Medium: A Review. *Water* **2023**, *15*, 81. [CrossRef]
31. Mishra, S.; Acharya, L.; Sharmila, S.; Sanjay, K.; Acharya, R. Designing G-C_3N_4/$NiFe_2O_4$ S-Scheme Heterojunctions for Efficient Photocatalytic Degradation of Rhodamine B and Tetracycline Hydrochloride. *Appl. Surf. Sci. Adv.* **2024**, *24*, 100647. [CrossRef]
32. Acharya, R.; Sillanpää, M.; Al-Farraj, S. A Comprehensive Review on Sequestration of Aqueous Cr (VI) over Graphene Based Adsorbents. *J. Hazard. Mater. Adv.* **2025**, *18*, 100670. [CrossRef]
33. Acharya, R.; Lenka, A.; Parida, K. Magnetite Modified Amino Group Based Polymer Nanocomposites towards Efficient Adsorptive Detoxification of Aqueous Cr (VI): A Review. *J. Mol. Liq.* **2021**, *337*, 116487. [CrossRef]
34. Adly, M.S.; El-Dafrawy, S.M.; El-Hakam, S.A. Application of Nanostructured Graphene Oxide/Titanium Dioxide Composites for Photocatalytic Degradation of Rhodamine B and Acid Green 25 Dyes. *J. Mater. Res. Technol.* **2019**, *8*, 5610–5622. [CrossRef]
35. Lee, S.-Y.; Park, S.-J. TiO_2 Photocatalyst for Water Treatment Applications. *J. Ind. Eng. Chem.* **2013**, *19*, 1761–1769. [CrossRef]
36. Tauc, J. Optical Properties and Electronic Structure of Amorphous Ge and Si. *Mater. Res. Bull.* **1968**, *3*, 37–46. [CrossRef]
37. Fuente, E.; Menéndez, J.A.; Díez, M.A.; Suárez, D.; Montes-Morán, M.A. Infrared Spectroscopy of Carbon Materials: A Quantum Chemical Study of Model Compounds. *J. Phys. Chem. B* **2003**, *107*, 6350–6359. [CrossRef]
38. Nguyen-Phan, T.-D.; Pham, V.H.; Shin, E.W.; Pham, H.-D.; Kim, S.; Chung, J.S.; Kim, E.J.; Hur, S.H. The Role of Graphene Oxide Content on the Adsorption-Enhanced Photocatalysis of Titanium Dioxide/Graphene Oxide Composites. *Chem. Eng. J.* **2011**, *170*, 226–232. [CrossRef]
39. Almeida, N.A.; Martins, P.M.; Teixeira, S.; Lopes da Silva, J.A.; Sencadas, V.; Kühn, K.; Cuniberti, G.; Lanceros-Mendez, S.; Marques, P.A.A.P. TiO_2/Graphene Oxide Immobilized in P(VDF-TrFE) Electrospun Membranes with Enhanced Visible-Light-Induced Photocatalytic Performance. *J. Mater. Sci.* **2016**, *51*, 6974–6986. [CrossRef]
40. Wang, G.; Guo, W.; Xu, D.; Liu, D.; Qin, M. Graphene Oxide Hybridised TiO_2 for Visible Light Photocatalytic Degradation of Phenol. *Symmetry* **2020**, *12*, 1420. [CrossRef]
41. Tang, B.; Chen, H.; Peng, H.; Wang, Z.; Huang, W. Graphene Modified TiO_2 Composite Photocatalysts: Mechanism, Progress and Perspective. *Nanomaterials* **2018**, *8*, 105. [CrossRef]
42. Kong, E.D.H.; Chau, J.H.F.; Lai, C.W.; Khe, C.S.; Sharma, G.; Kumar, A.; Siengchin, S.; Sanjay, M.R. GO/TiO_2-Related Nanocomposites as Photocatalysts for Pollutant Removal in Wastewater Treatment. *Nanomaterials* **2022**, *12*, 3536. [CrossRef]
43. Volfkovich, Y.M.; Rychagov, A.Y.; Sosenkin, V.E.; Baskakov, S.A.; Kabachkov, E.N.; Shulga, Y.M. Supercapacitor Properties of RGO-TiO_2 Nanocomposite in Two-Component Acidic Electrolyte. *Materials* **2022**, *15*, 7856. [CrossRef]
44. Tronox Ultrafine and Specialty Titanium Dioxide: CristalACTiVTM DT-51. Available online: https://www.tronox.com/product/cristalactiv-dt-51/ (accessed on 8 May 2025).
45. Ding, C.; Qin, X.; Tian, Y.; Cheng, B. PES Membrane Surface Modification via Layer-by-Layer Self-Assembly of GO@TiO_2 for Improved Photocatalytic Performance. *J. Memb. Sci.* **2022**, *659*, 120789. [CrossRef]
46. Utami, M.; Wang, S.; Fajarwati, F.I.; Salsabilla, S.N.; Dewi, T.A.; Fitri, M. Enhanced Photodegradation of Rhodamine B Using Visible-Light Sensitive N-TiO_2/RGO Composite. *Crystals* **2023**, *13*, 588. [CrossRef]
47. Bhattacharyya, S.; Donato, L.; Chakraborty, S.; Calabrò, V.; Davoli, M.; Algieri, C. Synergistic Efficiency of TiO_2-GO Nanocomposite Membranes in Dye Degradation for Sustainable Water Pollution Remedy. *Earth Syst. Environ.* **2025**, *9*, 639–652. [CrossRef]
48. Minella, M.; Sordello, F.; Minero, C. Photocatalytic Process in TiO_2/Graphene Hybrid Materials. Evidence of Charge Separation by Electron Transfer from Reduced Graphene Oxide to TiO_2. *Catal. Today* **2017**, *281*, 29–37. [CrossRef]
49. Guo, J.; Zhu, S.; Chen, Z.; Li, Y.; Yu, Z.; Liu, Q.; Li, J.; Feng, C.; Zhang, D. Sonochemical Synthesis of TiO_2 Nanoparticles on Graphene for Use as Photocatalyst. *Ultrason. Sonochem.* **2011**, *18*, 1082–1090. [CrossRef]
50. Stengl, V.; Bakardjieva, S.; Grygar, T.M.; Bludská, J.; Kormunda, M. TiO_2-Graphene Oxide Nanocomposite as Advanced Photocatalytic Materials. *Chem. Cent. J.* **2013**, *7*, 41. [CrossRef]
51. Nosaka, Y.; Nosaka, A.Y. Reconsideration of Intrinsic Band Alignments within Anatase and Rutile TiO_2. *J. Phys. Chem. Lett.* **2016**, *7*, 431–434. [CrossRef]
52. Gomez-Polo, C.; Larumbe, S.; Gil, A.; Muñoz, D.; Fernández, L.R.; Barquín, L.F.; García-Prieto, A.; Fdez-Gubieda, M.L.; Muela, A. Improved Photocatalytic and Antibacterial Performance of Cr Doped TiO_2 Nanoparticles. *Surf. Interfaces* **2021**, *22*, 100867. [CrossRef]
53. Abou-Gamra, Z.M.; Ahmed, M.A.; Hamza, M.A. Investigation of Commercial $PbCrO_4$/TiO_2 for Photodegradation of Rhodamine B in Aqueous Solution by Visible Light. *Nanotechnol. Environ. Eng.* **2017**, *2*, 12. [CrossRef]

54. Zhu, L.; Huang, D.; Ma, J.; Wu, D.; Yang, M.; Komarneni, S. Fabrication of AgBr/Ag_2CrO_4 Composites for Enhanced Visible-Light Photocatalytic Activity. *Ceram. Int.* **2015**, *41*, 12509–12513. [CrossRef]
55. Leong, C.Y.; Teh, H.L.; Chen, M.C.; Lee, S.L. Effect of Synthesis Methods on Properties of Copper Oxide Doped Titanium Dioxide Photocatalyst in Dye Photodegradation of Rhodamine B. *Sci. Technol. Indones.* **2022**, *7*, 91–97. [CrossRef]
56. Phuruanqrat, A.; Junsang, C.; Patiphatpanya, P.; Dumrongrojthanath, P.; Ekthammathat, N.; Karthik, A.; Thongtem, S.; Thongtem, T. Enhanced Visible-Light-Driven Photodegradation of Rhodamine B over $Ag_2C_2O_4$/Bi_2MoO_6 Nanocomposites. *J. Chem. Chem. Eng. Res. Artic.* **2020**, *39*, 29–37.
57. Avasthi, A.; Caro, C.; Pozo-Torres, E.; Leal, M.P.; García-Martín, M.L. *Magnetic Nanoparticles as MRI Contrast Agents*; Springer International Publishing: Berlin/Heidelberg, Germany, 2020; Volume 378, ISBN 0123456789.
58. Yu, L.; Xu, W.; Liu, H.; Bao, Y. Titanium Dioxide–Reduced Graphene Oxide Composites for Photocatalytic Degradation of Dyes in Water. *Catalysts* **2022**, *12*, 1340. [CrossRef]
59. Hidayat, R.; Wahyuningsih, S.; Fadillah, G.; Ramelan, A.H. Highly Visible Light Photodegradation of RhB as Synthetic Organic Dye Pollutant Over TiO_2-Modified Reduced Graphene Oxide. *J. Inorg. Organomet. Polym. Mater.* **2022**, *32*, 85–93. [CrossRef]
60. Hardiansyah, A.; Budiman, W.J.; Yudasari, N.; Isnaeni; Kida, T.; Wibowo, A. Facile and Green Fabrication of Microwave-Assisted Reduced Graphene Oxide/Titanium Dioxide Nanocomposites as Photocatalysts for Rhodamine 6G Degradation. *ACS Omega* **2021**, *6*, 32166–32177. [CrossRef]
61. Qu, X.; Hu, Q.; Song, Z.; Sun, Z.; Zhang, B.; Zhong, J.; Cao, X.; Liu, Y.; Zhao, B.; Liu, Z.; et al. Adsorption and Desorption Mechanisms on Graphene Oxide Nanosheets: Kinetics and Tuning. *Innovation* **2021**, *2*, 100137. [CrossRef]
62. Yang, X.; Wan, Y.; Zheng, Y.; He, F.; Yu, Z.; Huang, J.; Wang, H.; Ok, Y.S.; Jiang, Y.; Gao, B. Surface Functional Groups of Carbon-Based Adsorbents and Their Roles in the Removal of Heavy Metals from Aqueous Solutions: A Critical Review. *Chem. Eng. J.* **2019**, *366*, 608–621. [CrossRef]
63. Jahan, N.; Roy, H.; Reaz, A.H.; Arshi, S.; Rahman, E.; Firoz, S.H.; Islam, M.S. A Comparative Study on Sorption Behavior of Graphene Oxide and Reduced Graphene Oxide towards Methylene Blue. *Case Stud. Chem. Environ. Eng.* **2022**, *6*, 100239. [CrossRef]
64. Xiong, Q.; Zhang, F. Study on the Performance of Composite Adsorption of Cu^{2+} by Chitosan/β-Cyclodextrin Cross-Linked Zeolite. *Sustainability* **2022**, *14*, 2106. [CrossRef]
65. Yadav, A.; Yadav, M.; Gupta, S.; Popat, Y.; Gangan, A.; Chakraborty, B.; Ramaniah, L.M.; Fernandes, R.; Miotello, A.; Press, M.R.; et al. Effect of Graphene Oxide Loading on TiO_2: Morphological, Optical, Interfacial Charge Dynamics-A Combined Experimental and Theoretical Study. *Carbon N. Y.* **2019**, *143*, 51–62. [CrossRef]
66. Wang, R.; Shi, K.; Huang, D.; Zhang, J.; An, S. Synthesis and Degradation Kinetics of TiO_2/GO Composites with Highly Efficient Activity for Adsorption and Photocatalytic Degradation of MB. *Sci. Rep.* **2019**, *9*, 1–9. [CrossRef] [PubMed]
67. Siddeeg, S.M. A Novel Synthesis of TiO_2/GO Nanocomposite for the Uptake of Pb^{2+} and Cd^{2+} from Wastewater A Novel Synthesis of TiO_2/GO Nanocomposite for the Uptake of Pb^{2+} and Cd^{2+} from Wastewater. *Mater. Res. Express* **2020**, *7*, 025–038. [CrossRef]
68. Kaur, J.; Kaur, M. Facile Fabrication of Ternary Nanocomposite of $MgFe_2O_4$-TiO_2@GO for Synergistic Adsorption and Photocatalytic Degradation Studies. *Ceram. Int.* **2019**, *45*, 8646–8659. [CrossRef]
69. Joshi, N.C.; Congthak, R.; Gururani, P. Synthesis, Adsorptive Performances and Photo-Catalytic Activity of Graphene Oxide/TiO_2 (GO/TiO_2) Nanocomposite-Based Adsorbent. *Nanotechnol. Environ. Eng.* **2020**, *5*, 1–13. [CrossRef]
70. Jaramillo-Fierro, X.; Cuenca, G. Enhancing Methylene Blue Removal through Adsorption and Photocatalysis—A Study on the GO/$ZnTiO_3$/TiO_2 Composite. *Int. J. Mol. Sci.* **2024**, *25*, 4367. [CrossRef]
71. Xie, J.; Li, J.; Zhao, L.; Zhang, X.; Yu, B.; Wu, R.; Wang, R.; Liu, J.-H.; Xue, F.; Yang, S.-T. Fabrication of TiO_2-Graphene Oxide Aerogel for the Adsorption of Copper Ions. *Nanosci. Nanotechnol. Lett.* **2014**, *6*, 1018–1023. [CrossRef]